ACS APPLIED MATERIALS & INTERFACES

Research Article

www.acsami.org

Fast Direct Synthesis and Compaction of Homogenous Phase-Pure Thermoelectric Zn_4Sb_3

Hao Yin, Anders Bank Blichfeld, Mogens Christensen, and Bo Brummerstedt Iversen*

Centre for Materials Crystallography, Department of Chemistry and iNANO, Aarhus University, Langelandsgade 140, DK-8000 Aarhus C, Denmark

ABSTRACT: Zn_4Sb_3 is among the cheapest high performance thermoelectric materials, and it is made of relatively nontoxic elements. Strong activities are aimed at developing commercial power generation modules based on Zn_4Sb_3 making it vital to develop fast reliable synthesis processes for high-quality material. Here direct synthesis and compaction of homogeneous phase-pure thermoelectric Zn_4Sb_3 by spark plasma sintering (SPS) has been developed. Compared with the traditional quench and press method, the complexity and process time of the new method is very significantly reduced (order of magnitude), making large-scale production feasible. A composition gradient is observed in the pellet along the axis of applied pressure and current. The homogeneity of the pressed pellets is studied as a function of the SPS parameters: sintering time, applied current, sintering temperature and applied pressure, and the mechanism behind the formation of the gradient is discussed. The key finding is that pure and homogeneous Zn_4Sb_3 pellets can be produced by adding an extra layer of elemental Zn foil to compensate the Zn migration.

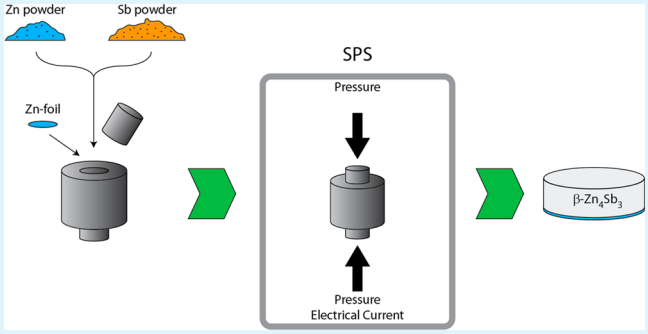

KEYWORDS: *thermoelectric materials, spark plasma sintering, zinc antimonide, Seebeck microprobe, powder X-ray diffraction*

INTRODUCTION

Increasing pressure on the environment and the energy supply has revived interest in the search for more efficient thermoelectric materials.[1−4] Thermoelectric materials are able to interconvert heat and electricity, and have huge potential in harvesting useful electricity from waste heat sources. One current focus is thermoelectric conversion of waste heat in motor vehicles, where the majority of the gasoline energy content is lost as heat. The β-phase of Zn_4Sb_3 is an excellent *p*-type thermoelectric semiconductor when used in the intermediate temperature range (473−673 K), which is exactly the region where many waste heat sources are available.[5] Good thermoelectric materials are typically heavily doped semiconductors with complex structures and large unit cells, which favor a high power factor ($S^2\sigma$, where S is the Seebeck coefficient and σ the electrical conductivity), while various phonon scattering processes reduces the thermal conductivity (κ).[2,6−9] In combination this leads to high thermoelectric figures of merit, $zT = S^2\sigma T/\kappa$, where T is the absolute temperature. In β-Zn_4Sb_3 three disordered interstitial Zn sites are believed to endow β-Zn_4Sb_3 with an unusually low thermal conductivity and make it a competitive candidate for thermoelectric applications,[2] although recent theoretical calculations have shown that the low thermal conductivity could be intrinsic also for the theoretically ordered Zn_6Sb_5.[10] Nevertheless, the presence of interstitial Zn still lowers the thermal conductivity.[11] β-Zn_4Sb_3 is also of interest, because it is among the cheapest thermoelectric materials known, and it is made of relatively nontoxic elements.[12,13] However, the instability of Zn_4Sb_3 in the working temperature range may limit its practical use in thermoelectric applications. β-Zn_4Sb_3 is known to degrade even below 500 K in air by the loss of Zn and growth of ZnSb, Sb and Zn (or its oxidation compound ZnO) as degradation products.[8,14−17] Recently a new window of stability for the β-Zn_4Sb_3 was discovered from 565 to 767 K, which might open up for further utilization of β-Zn_4Sb_3 at higher temperatures.[18]

Single-phase, polycrystalline β-Zn_4Sb_3 traditionally has been synthesized by thermally quenching a melted mixture of elemental Zn and Sb.[5] The synthesis takes several hours, plus time for weighing chemicals, evacuating and sealing quartz ampules, grinding presynthesized rods, sieving powders, and so on. Because of the significant microstrain generated by the large cooling rate, large crack-free and dense bulk materials are difficult to obtain. To meet the physical and mechanical requirements of a thermoelectric module, hot-pressing is necessary. However, pressing at elevated temperatures (>673 K) for several hours to achieve higher densities leads to substantial decomposition of Zn_4Sb_3. Iversen et al. found that the zT value decreased to just one-third of the original value after heating a quenched sample to 673 K because of the decomposition of Zn_4Sb_3 into ZnSb, Sb, and Zn.[16,19] Moreover,

Received: April 9, 2014
Accepted: June 6, 2014
Published: June 6, 2014

a pronounced difference in zT values indicates that a high density is a prerequisite for good thermoelectric performance.[20] The typical relative density of hot-pressed β-Zn_4Sb_3 pellets is 90−97%.[21−25] SPS pressing is another widely used pressing method, in which joule heat is generated by large pulsed direct current passing through the graphite pressing die and the material itself. The fast heating rate (up to 1000 degrees per minute) significantly reduces the duration of the pressing process.[26] Typical SPS pressing of Zn_4Sb_3 is carried out around 673 K for several minutes, accompanied by a pressure up to 100 MPa. Recently, it was reported that SPS pressing has a remarkable effect on the homogeneity and thermoelectric properties of Zn_4Sb_3 pellets.[27] Highly mobile Zn atoms migrate by the direct current and this leads to decomposition of the material and a compositional gradient along the pressing axis.[28] The control of Zn concentration/migration in β-Zn_4Sb_3 is crucial for obtaining the low thermal conductivity necessary for achieving a high zT, but also for obtaining stability on thermal cycling.[11] A method combining mechanical alloying with spark plasma sintering to obtain the sintered device of Zn_4Sb_3 was adopted by Takashi et al., and the mechanical allying processes was shown to be essential for the purity of the product.[29] In the present paper, systematic parametric studies on SPS pressing of Zn_4Sb_3 were carried out, where the homogeneity of the pellets is investigated in great detail using a potential Seebeck microprobe (PSM).[30,31] On the basis of the insight gained from these studies a novel one-step process combining the synthesis and the compaction of Zn_4Sb_3 using SPS is developed. The method is very time-saving compared with previous methods, which makes it attractive for commercial production of Zn_4Sb_3 pellets.[32]

EXPERIMENTAL SECTION

Zinc powder (99.99%, grain size <45 μm, MERCK KGaA) and antimony powder (99.5%, grain size <150 μm, SIGMA-Aldrich CHEMIE GmbH) were weighed with a molar ratio of 4:3. The powders were mixed in a ball mill mixer (SpectroMill, CHEMPLEX INDUSTRIES, INC) for 15 min. 2.5 g of the mixed powder was then loaded into a graphite die protected by BN spray with a diameter of 12.7 mm, and pressing was carried out using an SPS-515 instrument (SPS SYNTEX INC, Japan). The direction of the pulsed direct current is from the lower piston to the top piston in the instrument. The densities of the as-pressed discs were measured using Archimedes technique. Powder X-ray diffraction measurements (PXRD) were carried out on both sides of a gently polished pellet using a Rigaku Smartlab equipped with a Cu Kα source and parallel beam optics. The pellet was then cut horizontally through the middle so that the main body was also studied by PXRD using the same procedure. Scanning electron microscopy (SEM) and energy-dispersive X-ray spectroscopy (EDX) were obtained using a FEI NOVA 600 Nano SEM equipped with a TLD detector in secondary electron mode; all images were taken under high vacuum. The Zn compensated pellet used for SEM, EDX, and PXRD were made with 13 g of mixed powder and a graphite die with a diameter of 25.4 mm. Seebeck microprobe scanning was performed on the cross section of the pellets on a PANCO PSM.[30] During the PSM measurement, the sample surface is touched by a heated tungsten tip, which moves between measurements. This results in a spatially resolved map of the Seebeck coefficient with the resolution of ~100 μm.[30] The sample position is shown in Figure 1a. After the surface was polished, the pellet was sandwiched by two Ni pieces to make sure the whole width of the pellet was reachable by the tip.

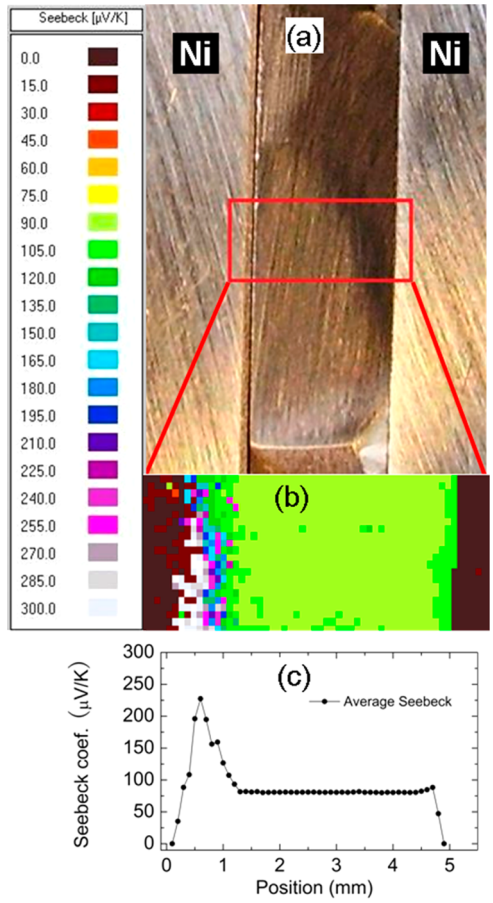

Figure 1. (a) Ni−Zn_4Sb_3−Ni sandwich for Seebeck microprobe scanning of Zn_4Sb_3 pressed at 673 K for 15 min with 100 MPa. The current direction is from the left to the right. Measured area is marked in red rectangular. (b) Seebeck microprobe scanning image. Local Seebeck coefficients are shown in colors using the color scale on the left. (c) Average Seebeck coefficient as a function of position on the pellet.

RESULTS AND DISCUSSION

The Seebeck microprobe scanning pattern of the sample pressed at 673 K for 15 min with 100 MPa is shown in Figure 1b. The dark areas on both sides correspond to Ni, which has a very low Seebeck coefficient at room temperature. The direction of the current during pressing was from the left to the right. Three distinct areas are seen on the cross section and the major area in the middle has a Seebeck coefficient around 90 μV/K, whereas the area close to the side where the current enters has significantly higher Seebeck coefficients (>200 μV/K). A thin layer on the opposite side has a Seebeck coefficient, which is higher than the main area (105−200 μV/K, green in the used color scale). As can be seen from the PXRD pattern in Figure 2, the main body of the pellet is the Zn_4Sb_3 phase, even though the Seebeck coefficient is slightly lower than reported in other studies[5,25,28,33−35] This is because the PSM method is less reliable for measuring absolute Seebeck values, whereas the technique is very strong for revealing relative changes. In Figure 1c, the Seebeck coefficients of the pixels that are in the same columns parallel to the sample surface are averaged and plotted as a function of position. To investigate the compositions on the two sides of the pellet, we carried out PXRD on the surface, see Figure 2. On the side where the current enters the pellet (the bottom of the pellet) ZnSb peaks are clearly seen, while on

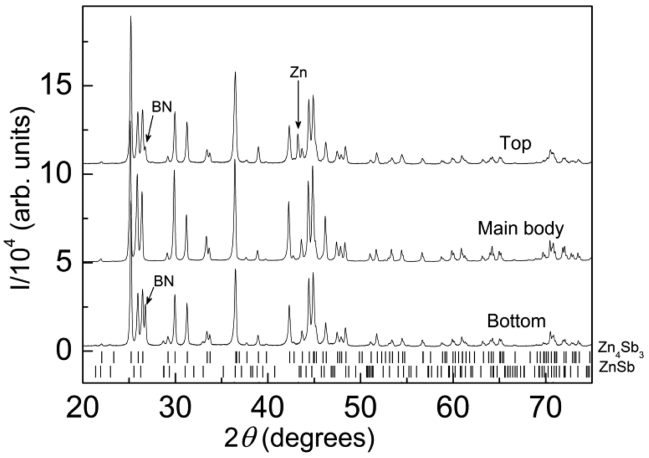

Figure 2. XRD patterns ($20 < 2\theta < 75°$) of the two sides and the main body of the SPS pressed pellet. The lower figure is the side where the current enters the pellet (bottom). ZnSb peaks are clearly seen. In the upper figure where the current leaves the pellet (top), Zn peak emerges ($2\theta = 43.3°$) with all the other peaks indexed to Zn_4Sb_3. Hexagonal BN remnant ($2\theta = 26.8°$) from SPS is recorded on both sides because the pellet was not well-polished in order to preserve as much sample as possible. All peaks from the main body can be indexed to Zn_4Sb_3.

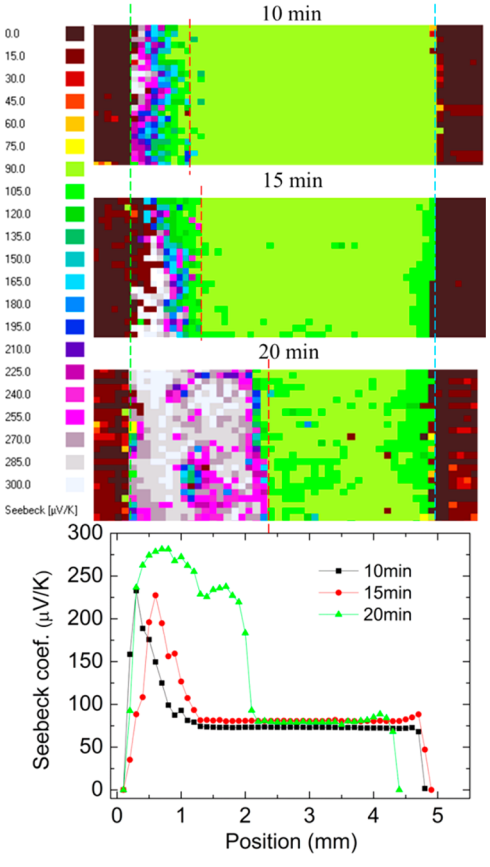

Figure 3. Seebeck microprobe scanning images of SPS pressed Zn_4Sb_3 with different sintering times. From the top to bottom t_s = 10, 15, and 20 min, respectively. The other SPS parameters were kept identical (t_{ramp} = 3 min, T = 673 K, and P = 100 MPa). The current direction is from the left to the right. Average Seebeck coefficients as a function of position are shown below.

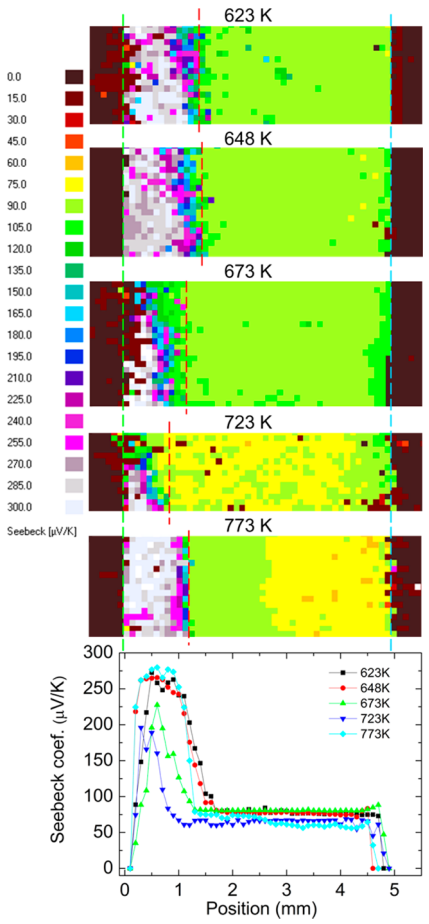

Figure 4. Seebeck microprobe scanning images of SPS pressed Zn_4Sb_3 pellets with different sintering temperatures. From the top T = 623, 648, 673, 723, and 773 K, respectively. The other SPS parameters were kept identical (t_{ramp} = 3 min, t_s = 15 min and P = 100 MPa). The current direction is from the left to the right.

the other side (the top of the pellet) they are hardly observable. This confirms previously reported observations, that Zn atoms migrate by the direct current of SPS and accumulate on the cathode, leaving ZnSb at the anode.[27] In the present study, a Zn peak is discernible in the PXRD pattern of the "green" area (top of the pellet), and the Seebeck coefficient on the corresponding area is higher than for the main body of the pellet (105−120 μV/K, see Figure 1). This is due to the decrease in the carrier concentration since the carriers (holes) of Zn_4Sb_3 are believed to be generated by Zn deficiency in the structure. Higher Zn content leads to enhanced Seebeck coefficient.[36] Recently, a new binary Zn_8Sb_7 phase was discovered and characterized, which has slightly higher Zn content.[37,38] However, because the symmetry of this phase is $P\bar{1}$ and the unit-cell parameters are relatively large, it is difficult to firmly identify whether the "green" phase is indeed the new phase. Hexagonal BN remnant ($2\theta = 26.8°$) from the SPS pressing is observed on both sides, because the pellet was only gently polished to preserve as much sample as possible. In the following paragraphs the homogeneity of the pellets is investigated separately as a function of the following SPS parameters: sintering time (t_s), sintering temperature (T), applied pressure (P), and applied current (tuned by heating rate, corresponding to heating ramp time t_{ramp}). The pellet pressed with a heating ramp time of 3 min to 673 K for 15 min with 100 MPa is considered a

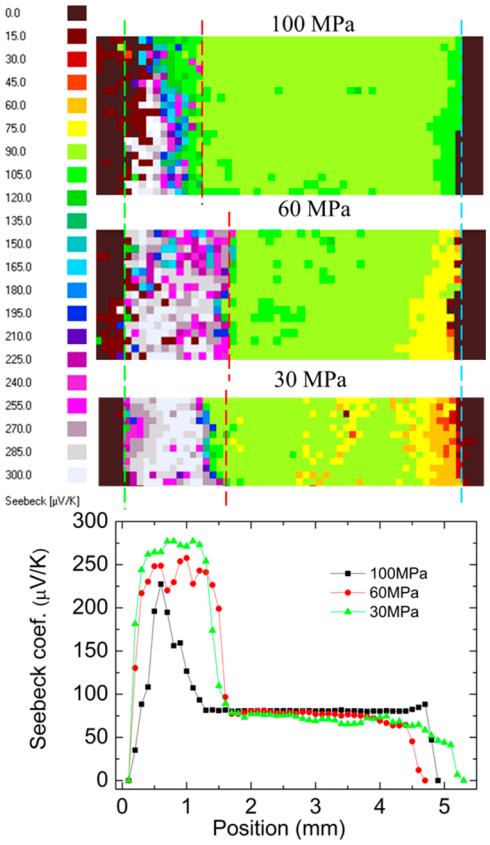

Figure 5. Seebeck microprobe scanning images of SPS pressed Zn_4Sb_3 pellets with different applied pressure. From the top P = 100, 60, and 35 MPa, respectively. The other SPS parameters were kept identical (t_{ramp} = 3 min, t_s = 15 min, and T = 673 K). The current direction is from the left to the right.

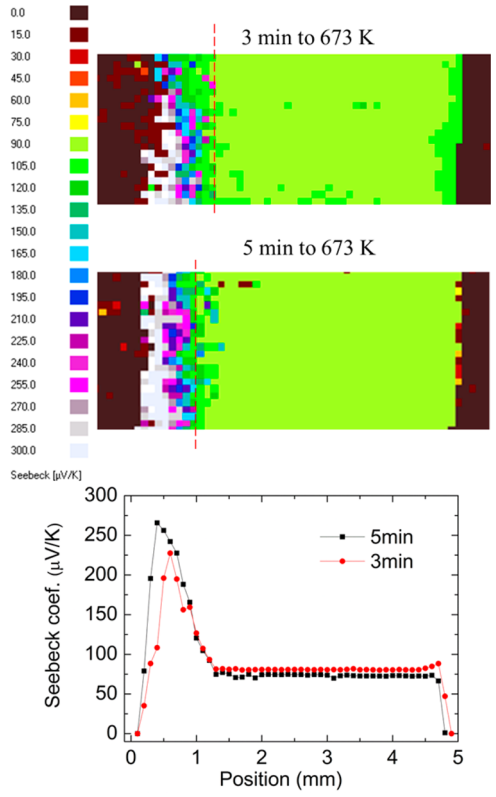

Figure 6. Seebeck microprobe scanning patterns of SPS pressed Zn_4Sb_3 with different heating rate (applied current). From top: t_{ramp} = 3 and 5 min. Other parameters are kept unchanged (t_s = 15 min, T = 673 K, and P = 100 MPa). The current direction is from the left to the right.

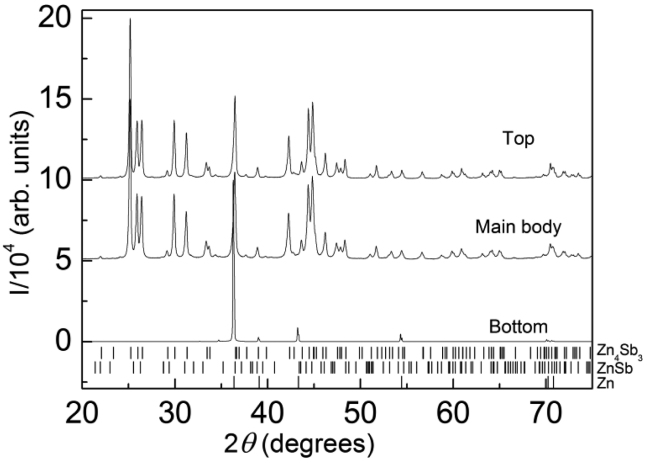

Figure 7. XRD patterns ($20 < 2\theta < 75°$) of the two sides and the main body of the SPS pressed pellet with a Zn-foil at the bottom. All the other SPS parameters were kept identical (t_{ramp} = 3 min, t_s = 15 min, T = 673 K, and P = 100 MPa). The lower figure is the side where the current enters the pellet (bottom). Only peaks from the Zn foil are seen. All peaks from the main body and the top surface can be indexed to Zn_4Sb_3.

reference. All PSM images are normalized in width for comparison. Seebeck coefficients of the pixels in the same column that is parallel to the sample surface are averaged and plotted as a function of position.

Sintering Time. Figure 3 shows the Seebeck microprobe scanning images of SPS pellets pressed with sintering times of 10, 15, and 20 min, respectively. The heating ramp was kept unchanged, i.e. heating from room temperature to 673 K within 3 min (t_{ramp} = 133 K/min). The applied pressure (P) was 100 MPa. The relative densities of the three samples are higher than 99% relative to 6.39 g/cm^3 of Zn_4Sb_3. It is worth mentioning that even though the pellets are multiphased, then the density of the main impurity ZnSb is accidentally the same as for Zn_4Sb_3. This means that the overall density of the pellet still reflects the density of the Zn_4Sb_3 phase. In Figure 3, dashed lines are guides to the eye to allow comparison of the width of each phase. Significant increases in the widths of both the ZnSb phase on the left side, and the "green" phase on the right side are noticeable with the increasing sintering time. This indicates a more severe decomposition of Zn_4Sb_3. Moreover, the homogeneity of the main Zn_4Sb_3 phase deteriorates, which is revealed by the emergence and increase of the "green" phase. Clearly, longer sintering time leads to more severe degradation of the pellet. Ten minutes is sufficient for directly synthesizing Zn_4Sb_3 from elemental Zn and Sb by SPS using the present apparatus and size of the die. Prolonging the sintering time to 15 or 20 min only deteriorates the homogeneity of the pellets.

Sintering Temperature. Five pellets were sintered at different temperatures (T = 623, 648, 673, 723, and 773 K) with identical heating ramp, holding time and pressure (t_{ramp} = 3 min, t_s = 15 min, and P = 100 MPa). The relative density of the pellet sintered at the lowest temperature is approximately 95%, whereas the other pellets are very close to 100% density.

dx.doi.org/10.1021/am502089a | ACS Appl. Mater. Interfaces 2014, 6, 10542−10548

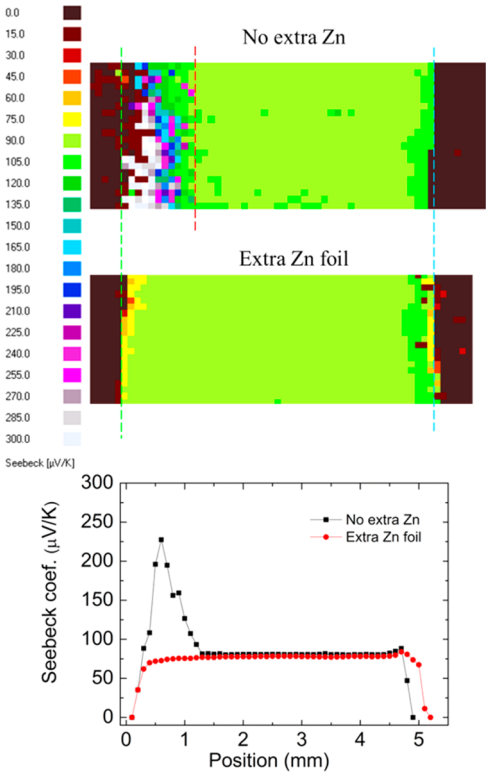

Figure 8. Seebeck microprobe scanning images of SPS pressed Zn_4Sb_3 pellets with and without extra Zn foil on the left side. All the other SPS parameters were kept identical (t_{ramp} = 3 min, t_s = 15 min, T = 673 K, and P = 100 MPa). The current direction is from the left to the right.

Surprisingly, lowering of the sintering temperature does not lead to less decomposition of Zn_4Sb_3 as seen in Figure 4. Compared with the sample sintered at 673 K, more ZnSb impurity phase emerges in the two samples sintered at 623 and 648 °C. Thus, the decomposition of Zn_4Sb_3 depends less on the temperature during direct synthesis by SPS. When sintered at temperatures above 673 K, the width of ZnSb phase does not increase pronouncedly. However, the homogeneity of the main phase deteriorates noticeably by the emergence of another phase with lower Seebeck coefficient shown in yellow on the used color scale. Dasgupta et al. suggested that this is a mixture of zinc deficient Zn_4Sb_3 and Zn.[28] When sintered at 773 K, the "yellow" phase accumulates on the right. This confirms that the inhomogeneity of the pellet is due to the migration of Zn along the axis of the pressing.[27] The mobility of Zn increases with the increasing temperature, which makes the migration faster.

Applied Pressure. The effect of the applied pressure on the degradation of Zn_4Sb_3 is shown in Figure 5. Both pellets sintered under pressures of 60 and 30 MPa decompose more significantly than the one pressed under 100 MPa. At low pressure, more ZnSb as well as the "yellow" phase are formed at the sides of the pellets. This may be because there is less contact between grains at lower pressure, which increases the resistivity of the sample. Thus, more joule heat is generated during sintering, which accelerates the decomposition. The pellet pressed with 30 MPa even broke into pieces after pressing. For this pellet, the estimated density was less than 89% of the theoretical density, indicating a deteriorated mechanical property.

Applied Current. Since the heat is generated internally by the current passing through the sample, the effect of the applied current through the material during heating may be investigated by changing the heating ramp. Figure 6 shows the influence of the applied current (heating ramp) on the phase homogeneity of the pellets. All the other parameters are kept identical (t_s = 15 min, T = 673 K, and P = 100 MPa). When the sample is heated to 673 K within 3 min (t_{ramp} = 133 K/min), the applied current is approximately 300 A. It decreases to around 200 A when the heating ramp is prolonged to 5 min (t_{ramp} = 80 K/min). Lower current leads to enhanced homogeneity of the pellet. This confirms the transporting effect of the current in the migration of Zn during SPS.[27] The densities of the two pellets were measured to be over 99%.

Extra Zn. Several studies have suggested that methods should be developed to compensate for the Zn lost in synthesis and pressing of Zn_4Sb_3 in order to improve the properties.[16,28] An extra 0.10 mm thick Zn foil was added to the bottom of the pressing assembly where the current enters the pellet with the intention to compensate the Zn lost at the cathode. Remarkably, no ZnSb phase is observed after sintering with the extra Zn foil present, see Figure 7. Only a thin layer of "yellow" phase is formed as seen in Figure 8. This not only indicates that the formation of ZnSb phase in the other pellets

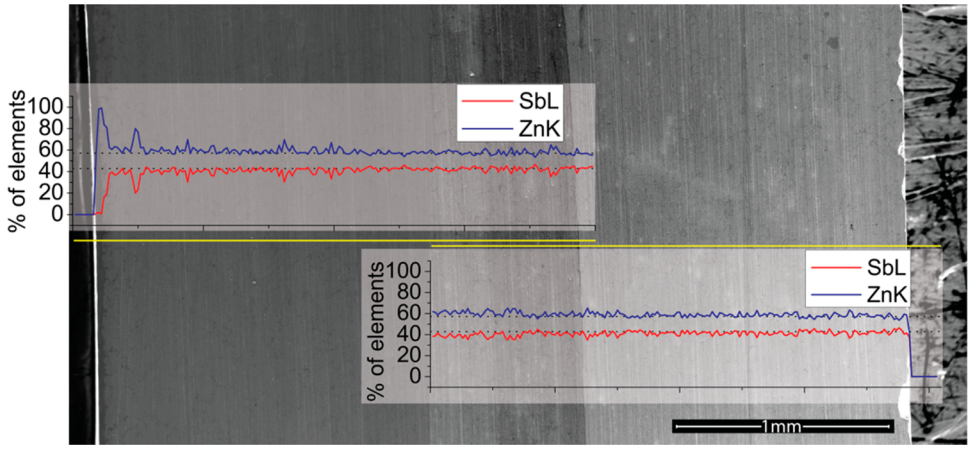

Figure 9. Two EDX line scans show that the overall composition of the SPS pressed Zn_4Sb_3 pellets with and without extra Zn foil corresponds to Zn:Sb = 4:3, except at the right side where the Zn-foil is placed. The SEM picture is a merge of two individual pictures, and the line in the middle stems from the polishing.

is due to the lost Zn, but it also confirms that the "yellow" phase appearing on the right side is a Zn-rich phase or a mixture of phases containing Zn. Compared with the pellet pressed without extra Zn, the pellet with Zn foil is homogeneous and phase pure as seen from the PXRD in Figure 7 and EDX line scan in Figure 9. The density of the pellet is very close to that of Zn_4Sb_3. This demonstrates that homogeneous phase pure Zn_4Sb_3 pellets with high density can be synthesized directly in the SPS in a matter of minutes rather than the six to 8 h needed for traditional synthesis and pressing methods. The Zn compensated pellet used for PXRD and EDX was produced in a scale-up synthesis compared with the rest of the pellets used in this study. The present approach provides a facile method for large-scale production of phase pure Zn_4Sb_3 pellets with high density for potential commercial applications.

CONCLUSION

A one-step direct synthesis and pressing process of Zn_4Sb_3 using SPS is explored. Dense pellets are obtained (relative density >99%). Since the duration of the sintering at elevated temperatures is reduced remarkably compared to hot-press, the decomposition of Zn_4Sb_3 is limited. However, the direct current in SPS promotes the migration of Zn and thus accelerates the decomposition, when high heating rates are used. Addition of a Zn foil to compensate for Zn lost during sintering produces a dense, phase pure, and homogeneous Zn_4Sb_3 pellet. Compared with the traditional method involving quenching and pressing, direct synthesis is easier and much faster. The whole process takes less than 30 min, which is preferable for large scale production of Zn_4Sb_3. In general, direct SPS synthesis pressing possibly may be extended to other metastable materials to produce dense products within a relatively short time.

AUTHOR INFORMATION

Corresponding Author

*E-mail: bo@chem.au.dk.

Notes

The authors declare no competing financial interest.

ACKNOWLEDGMENTS

This work was supported by the Danish National Research Foundation (Center for Materials Crystallography, DNRF93), and the Danish Strategic Research Council (Center for Energy Materials). The PhD stipend for A.B.B. is partly funded by SINO Danish Center. We thank Dr. Jeff G. Snyder for fruitful discussions.

REFERENCES

(1) Sootsman, J. R.; Chung, D. Y.; Kanatzidis, M. G. New and Old Concepts in Thermoelectric Materials. *Angew. Chem., Int. Ed.* **2009**, *48*, 8616−8639.

(2) Snyder, G. J.; Christensen, M.; Nishibori, E.; Caillat, T.; Iversen, B. B. Disordered Zinc in Zn_4Sb_3 with Phonon-glass and Electron-crystal Thermoelectric Properties. *Nat. Mater.* **2004**, *3*, 458−463.

(3) Iversen, B. B. Fulfilling Thermoelectric Promises: β-Zn_4Sb_3 From Materials Research to Power Generation. *J. Mater. Chem.* **2010**, *20*, 10778−10787.

(4) Christensen, M.; Johnsen, S.; Iversen, B. B. Thermoelectric Clathrates of Type I. *Dalton Trans.* **2010**, *39*, 978−992.

(5) Caillat, T.; Fleurial, J. P.; Borshchevsky, A. Preparation and Thermoelectric Properties of Semiconducting Zn_4Sb_3. *J. Phys. Chem. Solids* **1997**, *58*, 1119−1125.

(6) Caillat, T.; Borshchevsky, A.; Fleurial, J.-P. US Patent 6942728 B2. 6942728 B2, 2005.

(7) Cargnoni, F.; Nishibori, E.; Rabiller, P.; Bertini, L.; Snyder, G. J.; Christensen, M.; Gatti, C.; Iversen, B. B. Interstitial Zn Atoms Do the Trick in Thermoelectric Zinc Antimonide, Zn_4Sb_3: A Combined Maximum Entropy Method X-Ray Electron Density and Ab Initio Electronic Structure Study. *Chem. - Eur. J.* **2004**, *10*, 3861−3870.

(8) Mozharivskyj, Y.; Janssen, Y.; Harringa, J. L.; Kracher, A.; Tsokol, A. O.; Miller, G. J. $Zn_{13}Sb_{10}$: A Structural and Landau theoretical Analysis of Its Phase Transitions. *Chem. Mater.* **2006**, *18*, 822−831.

(9) Snyder, G. J.; Toberer, E. S. Complex Thermoelectric Materials. *Nat. Mater.* **2008**, *7*, 105−114.

(10) Bjerg, L.; Iversen, B. B.; Madsen, G. K. H. Modeling the Thermal Conductivities of the Zinc Antimonides ZnSb and Zn_4Sb_3. *Phys. Rev. B: Condens. Matter Mater. Phys.* **2014**, *89*, 024304.

(11) Dasgupta, T.; Stiewe, C.; Sesselmann, A.; Yin, H.; Iversen, B. B.; Mueller, E. Thermoelectric Studies in β-Zn_4Sb_3—The Complex Interdependence Between Thermal Stability, Thermoelectric Transport, and Zinc Content. *J. Appl. Phys.* **2013**, *113*, 103708.

(12) Nylen, J.; Andersson, M.; Lidin, S.; Haussermann, U. The Structure of α-Zn_4Sb_3: Ordering of the Phonon-Glass Thermoelectric Material β-Zn_4Sb_3. *J. Am. Chem. Soc.* **2004**, *126*, 16306−16307.

(13) Ur, S. C.; Nash, P.; Schwarz, R. Mechanical and Thermoelectric Properties of Zn_4Sb_3 and Zn_4Sb_3+Zn Directly Synthesized Using Elemental Powders. *Met. Mater. Int.* **2005**, *11*, 435−441.

(14) Pedersen, B. L.; Iversen, B. B. Thermally Stable Thermoelectric Zn_4Sb_3 by Zone-Melting Synthesis. *Appl. Phys. Lett.* **2008**, *92*, 161907.

(15) Zhang, L. T.; Tsutsui, M.; Ito, K.; Yamaguchi, M. Effects of ZnSb and Zn Inclusions on the Thermoelectric Properties of β-Zn_4Sb_3. *J. Alloys Compd.* **2003**, *358*, 252−256.

(16) Iversen, B. B.; Lundtoft, B.; Christensen, M.; Platzek, D. WO Patent. 128467 A2, 2006.

(17) Birkel, C. S.; Claudio, T.; Panthöfer, M.; Birkel, A.; Koll, D.; Kieslich, G.; Schmidt, J.; Hermann, R.; Tremel, W. Properties of Spark Plasma Sintered Nanostructured $Zn_{1+x}Sb$. *Phys. Status Solidi A* **2011**, *208*, 1913−1919.

(18) Lin, J.; Li, X.; Qiao, G.; Wang, Z.; Carrete, J.; Ren, Y.; Ma, L.; Fei, Y.; Yang, B.; Lei, L.; Li, J., Unexpected High-Temperature Stability of β-Zn_4Sb_3 Opens the Door to Enhanced Thermoelectric Performance. *J. Am. Chem. Soc.* **2014**.

(19) Yin, H.; Pedersen, B. L.; Iversen, B. B. Thermal Stability of High Performance Thermoelectric β-Zn_4Sb_3 in Argon. *Eur. J. Inorg. Chem.* **2011**, 2733−2737.

(20) Pedersen, B. L.; Birkedal, H.; Iversen, B. B.; Nygren, M.; Frederiksen, P. T. Influence of Sample Compaction on the Thermoelectric Performance of Zn_4Sb_3. *Appl. Phys. Lett.* **2006**, *89*, 242108.

(21) Caillat, T.; Fleurial, J. P.; Borshchevsky, A. A Low thermal conductivity Compound For Thermoelectric Applications: β-Zn_4Sb_3. *Proceedings Ict '96 - Fifteenth International Conference on Thermoelectrics* **1996**, 151−154.

(22) Zhu, T. J.; Zhao, X. B.; Hu, S. H.; Wu, Z. T.; Zhou, B. C. Transport Properties of a New Type of Thermoelectric Material β-Zn_4Sb_3. *Rare Met. Mater. Eng.* **2001**, *30*, 187−189.

(23) Ur, S. C.; Nash, P.; Kim, I. H. Solid-State Syntheses and Properties of Zn_4Sb_3 Thermoelectric Materials. *J. Alloys Compd.* **2003**, *361*, 84−91.

(24) Ueno, K.; Yamamoto, A.; Noguchi, T.; Inoue, T.; Sodeoka, S.; Takazawa, H.; Lee, C. H.; Obara, H. Optimization of Hot-Press conditions of Zn_4Sb_3 for High Thermoelectric Performance - I. Physical Properties and Thermoelectric Performance. *J. Alloys Compd.* **2004**, *384*, 254−260.

(25) Souma, T.; Nakamoto, G.; Kurisu, M. Low-Temperature Thermoelectric Properties of α- and β-Zn_4Sb_3 Bulk Crystals Prepared by a gradient Freeze Method and a Spark Plasma Sintering Method. *J. Alloys Compd.* **2002**, *340*, 275−280.

(26) Munir, Z. A.; Anselmi-Tamburini, U.; Ohyanagi, M. The Effect of Electric field and Pressure on the Synthesis and Consolidation of

Materials: A Review of the Spark Plasma Sintering Method. *J. Mater. Sci.* **2006**, *41*, 763−777.
(27) Yin, H.; Christensen, M.; Lock, N.; Iversen, B. B. Zn Migration During Spark Plasma Sintering of Thermoelectric Zn_4Sb_3. *Appl. Phys. Lett.* **2012**, *101*, 043901.
(28) Dasgupta, T.; Stiewe, C.; Boettcher, L.; Hassdorf, R.; Yin, H.; Iversen, B.; Mueller, E. Multiple Phase Formation and Its Influence on Lattice Thermal Conductivity in β-Zn_4Sb_3. *J. Mater. Res.* **2011**, *26*, 1925−1932.
(29) Takashi, I.; Jiayi, S.; Kuniyuki, K., Thermoelectric Properties of β-Zn_4Sb_3 Synthesized by MA-SPS Method. In *2nd International Energy Conversion Engineering Conference*; Providence, RI, Aug 18, 2004 ; American Institute of Aeronautics and Astronautics: Reston, VA, 2004.
(30) Platzek, D.; Karpinski, G.; Stiewe, C.; Ziolkowski, P.; Drasar, C.; Muller, E. Potential-Seebeck-Microprobe (PSM): Measuring the Spatial Resolution of the Seebeck Coefficient and the Electric Potential. In *24th International Conference on Thermoelectrics (ICT)*; Clemson, SC, June 19−23, 2005 ; IEEE: Piscataway, NJ, 2005; pp 13−16.
(31) Ziolkowski, P.; Karpinski, G.; Dasgupta, T.; Muller, E. Probing Thermopower on the Microscale. *Phys. Status Solidi A* **2013**, *210*, 89−105.
(32) Iversen, B. B.; Christensen, M.; Yin, H. WO patent. 010547 A1, 2013.
(33) Ur, S. C.; Kim, I. H.; Nash, P. Thermoelectric Properties of Zn_4Sb_3 Directly Synthesized by Hot Pressing. *Mater. Lett.* **2004**, *58*, 2132−2136.
(34) Zhu, T. J.; Zhao, X. B.; Yan, M.; Hu, S. H.; Li, T.; Zhou, B. C. Transport Properties of β-Zn_4Sb_3 Prepared by Vacuum Melting. *Mater. Lett.* **2000**, *46*, 44−48.
(35) Pedersen, B. L.; Yin, H.; Birkedal, H.; Nygren, M.; Iversen, B. B. Substitution in $M_xZn_{4-x}Sb_3$: Effect on Thermal Stability, Crystal Structure, Phase Transitions, and Thermoelectric Performance. *Chem. Mater.* **2010**, *22*, 2375−2383.
(36) Toberer, E. S.; Rauwel, P.; Gariel, S.; Tafto, J.; Snyder, G. J. Composition and the Thermoelectric Performance of β-Zn_4Sb_3. *J. Mater. Chem.* **2010**, *20*, 9877−9885.
(37) Birkel, C. S.; Mugnaioli, E.; Gorelik, T.; Kolb, U.; Panthöfer, M.; Tremel, W. Solution Synthesis of a New Thermoelectric $Zn_{1+x}Sb$ Nanophase and Its Structure Determination Using Automated Electron Diffraction Tomography. *J. Am. Chem. Soc.* **2010**, *132*, 9881−9889.
(38) Pomrehn, G. S.; Toberer, E. S.; Snyder, G. J.; van de Walle, A. Predicted Electronic and Thermodynamic Properties of a Newly Discovered Zn_8Sb_7 Phase. *J. Am. Chem. Soc.* **2011**, *133*, 11255−11261.